Energy 346 (2026) 140252

Contents lists available at ScienceDirect

Energy

journal homepage: www.elsevier.com/locate/energy

Data-driven voltage control for dual-mode power regulation in small wind turbines

Jesus Clavijo-Camacho *, Reyes S. Herrera, Francisco J. Ruiz-Rodriguez, Juan P. Torreglosa

Department of Electrical Engineering of University of Huelva, Huelva, Spain

ARTICLE INFO

Keywords:
Power control management
MPPT
Power curtailment
Small wind turbines
DC-DC boost converter

ABSTRACT

Wind energy is a key renewable resource for sustainable power generation, with small-scale Wind Energy Conversion Systems (WECS) playing an increasingly important role in distributed generation. This paper presents a novel sensorless, voltage-based power control strategy for small wind turbines equipped with Permanent Magnet Synchronous Generators (PMSG), enabling operation in different modes: Maximum Power Point Tracking (MPPT) or dynamic power curtailment. The proposed method uses predefined Lookup Table (LUT)-based characterization, mapping wind speed, generator voltage, and power output, allowing real-time selection of the optimal voltage reference depending on the controller's mode. The control is implemented through a cascaded PI-based structure, regulating power delivery by adjusting the generator's electrical load via a DC-DC boost converter. The system supports three modes for variable wind speed: (1) extracting maximum available power (MPPT), (2) maintaining a percentage of power reserve, or (3) regulating active power delivery. This flexibility enables the system to adapt to external demands, whether for grid support or standalone operation. The method is validated through simulation and experimental testing, demonstrating stable operation, fast response to setpoint changes, and scalability to higher power levels. These results confirm the feasibility of integrating small wind turbines into ancillary services, enhancing their role in grid-support applications.

List of Symbols and Abbreviations

Symbol	Description	Unit	Symbol	Description	Unit
P_w	Total available wind power	W	T_e	Electromagnetic torque generated by the PMSG	N·m
P_m	Mechanical power extracted by the wind turbine	W	J	Total rotational inertia of turbine and generator	kg·m^2
P_e	Electrical power output of generator	W	p	Number of pole pairs of generator	–
P_{MAX}	Maximum available electrical power at given wind speed	W	ϕ	Magnetic flux linkage from permanent magnets	Wb
P_{ref}	Reference electrical power	W	i_d, i_q	Stator current components in d–q reference frame	A
$P_{reserve}$	Power reserve	W	v_d, v_q	Stator voltage components in d–q reference frame	V
$P_{(V_i,v_j)}$	Electrical power measured for voltage V_i and wind speed v_j (LUT element)	W	R	Stator phase resistance	Ω
ρ	Air density	kg·m^{-3}	L_d, L_q	Stator inductances in d and q axes	H

(continued on next column)

(continued)

(continued on next page)

* Corresponding author.
E-mail address: jesus.clavijo@die.uhu.es (J. Clavijo-Camacho).

https://doi.org/10.1016/j.energy.2026.140252
Received 24 April 2025; Received in revised form 13 January 2026; Accepted 28 January 2026
Available online 29 January 2026

(*continued*)

Symbol	Description	Unit	Symbol	Description	Unit
S	Swept area of turbine blades	m^2	$V_{generator}$	Generated RMS voltage at generator terminals	V
R_b	Radius of turbine blades	m	V_{in}	Input voltage to DC/DC boost converter (rectifier output)	V
v_w	Wind speed (incident velocity)	$m{\cdot}s^{-1}$	$V_{DC\ bus}$	DC bus voltage (output of converter)	V
$v_{cut\text{-}in}$	Cut-in wind speed	$m{\cdot}s^{-1}$	V_{ref}	Voltage reference determined by control system	V
$v_{cut\text{-}off}$	Cut-off wind speed	$m{\cdot}s^{-1}$	D	Duty cycle of the DC/DC boost converter	–
λ	Tip speed ratio	–	I_{in}	Inductor current (input current to converter)	A
β	Pitch angle of blades	°	I_{out}	Output current from converter	A
$C_P(\lambda,\beta)$	Power coefficient (aerodynamic efficiency factor)	–	$e_1(t)$	Voltage error signal	V
ω_m	Mechanical angular velocity of the turbine rotor	$rad{\cdot}s^{-1}$	$e_2(t)$	Current error signal	A
T_m	Mechanical torque produced by the turbine	N·m	$u_1(t)$	Control output of voltage loop (outer loop)	V
$u_2(t)$	Control output of current loop (inner loop, PWM signal)	–	t_{resp}	Response time to reach steady-state after power setpoint change	s
K_{p1}, K_{i1}	Proportional and integral gains of outer voltage loop	–	$\%_{reserve}$	Power curtailment percentage (reserve fraction)	%
K_{p2}, K_{i2}	Proportional and integral gains of inner current loop	–	L	Converter inductance	H
f_{PWM}	Switching frequency of the PWM signal	Hz	C	Converter output capacitor	F
k	Generator voltage constant	$V{\cdot}s{\cdot}rad^{-1}$	C_{rip}	Rectifier-side smoothing capacitor	F

1. Introduction

Wind energy has become one of the leading renewable electricity sources worldwide. In 2024, renewables accounted for 46.9 % of the European Union's electricity generation, with wind power contributing 39 % of this renewable share [1]. This progress aligns with the European Union's climate objectives and the targets set within the 2030 Agenda for Sustainable Development, which promote the large-scale integration of clean energy [2]. This sustained growth is supported by technological advances and policy incentives, encouraging deployment from large offshore projects to distributed generation. Altogether, these developments underline the increasing relevance of wind power as a key pillar in the global energy transition.

Within this landscape, small wind turbines (SWT) (<100 kW) are gaining traction, particularly in distributed generation and remote applications [3–5]. For instance, rural electrification projects in Northern Europe and hybrid renewable systems in isolated islands or farms increasingly rely on SWTs to complement solar generation, reducing diesel dependency and improving local energy autonomy [6]. Recent reports from the U.S. Department of Energy estimate that distributed wind installations surpassed 1.1 GW of cumulative capacity in 2023 [7], with small wind systems representing a growing share of new projects. These systems offer advantages such as reduced transmission losses and enhanced local energy resilience, making them an attractive option for decentralized energy solutions. However, effective grid integration of SWTs. requires advanced control strategies that optimize power extraction while ensuring system stability [8].

This paper presents a sensorless voltage-based control strategy for small wind turbines, enabling both Maximum Power Point Tracking (MPPT) and dynamic power curtailment. The approach provides an efficient framework for regulating power extraction in grid-connected and standalone modes, facilitating the integration of SWTs into distributed and ancillary service applications. Simulation and experimental validation confirm its simplicity, adaptability, and effectiveness for small-scale renewable systems.

1.1. State of art

Control strategies in Wind Energy Conversion System (WECS) can be broadly classified based on their regulation approach, which may focus on either Maximum Power Point Tracking (MPPT) [9–12] or power curtailment management [13–15], depending on operational objectives. These control methods rely on three main techniques: **(i) Pitch angle control** [16], which adjusts the blade orientation to regulate aerodynamic efficiency [17]—widely used in large-scale turbines but often impractical in small-scale systems due to cost and mechanical constraints; **(ii) Torque control** [18,19], which modifies the generator's electromagnetic torque to regulate rotational speed and optimize energy extraction, commonly implemented in both large and medium-scale wind turbines; and **(iii) Converter-side control** [20,21], where power electronics—such as DC-DC converters or back-to-back AC-DC-AC converters—adjust the electrical operating point to achieve the desired power regulation.

While large-scale wind turbines can implement MPPT and power reserve strategies through any of these control techniques, SWTs are typically limited to converter-side control due to their fixed-speed and direct-drive configurations [22]. Among these, Permanent Magnet Synchronous Generators (PMSG) are widely adopted in SWTs [23,24] due to their high efficiency and reliability, but their lack of active mechanical control necessitates power regulation exclusively through electrical means. Although MPPT strategies are extensively studied, power curtailment control in SWTs remains underexplored, despite its growing importance for grid integration and ancillary services.

Since SWTs rely solely on **(iii) Converter-side control**, power regulation is typically managed through cascaded PI/PID controllers, which remain the standard choice due to their simplicity, robustness, and ease of implementation in both grid-connected and standalone configurations [25]. However, in pursuit of greater adaptability and improved disturbance rejection, alternative strategies have been explored. Among them, fuzzy logic control [26] has gained attention for its ability to handle nonlinearities without requiring an explicit mathematical model, though at the cost of extensive parameter tuning. Similarly, sliding mode control [27] offers strong robustness against uncertainties but tends to introduce high-frequency switching effects, which can be detrimental in power electronics applications. A more predictive approach can be found in model predictive control [28,29], which dynamically adjusts control actions by forecasting system behaviour, optimizing performance in real time. While this method is highly effective, its computational burden often makes it less practical for SWTs with limited processing resources. Ultimately, the choice of control strategy depends on the specific operational constraints of the system, balancing complexity, responsiveness, and efficiency.

Another key area in converter-based power control is the development of grid-support strategies that enhance the stability and reliability

of the electrical system. These methods regulate power output based on frequency stabilization, power factor correction (P/Q control) [30], or active/reactive power dispatch [31], ensuring better integration of WECS into modern grids. Among these, Direct Power Control [32] regulates instantaneous active and reactive power without requiring modulation, offering fast dynamic response but at the expense of higher implementation complexity. Virtual inertia emulation enables WECS to mimic the inertial response of conventional synchronous generators [33, 34], helping stabilize grid frequency by dynamically adjusting power injection based on grid fluctuations. While these techniques enhance grid stability and support ancillary services, they become ineffective in isolated systems where frequency regulation is not a priority or when there is no external grid reference. In standalone applications, power control shifts towards load-following strategies, where the turbine's output is adjusted based on local demand rather than external frequency or power factor constraints [35]. This fundamental difference highlights the need for the proposed adaptable control methodology that can operate both in grid-connected and isolated scenarios, ensuring reliable power management across different network configurations.

A few studies have explicitly explored power control strategies operating beyond MPPT in SWTs. In Ref. [36], the authors propose an inverter-based control strategy incorporating battery storage as backup, which adds complexity and cost—an aspect not required in the present work. Another method, presented in Ref. [37], merges converter and inverter control to regulate injected power but lacks experimental validation and requires a dedicated inverter for each μgrid generator system.

Table 1 summarizes that most existing studies on SWT control focus solely on MPPT operation or rely on inverter-based curtailment requiring auxiliary hardware. In contrast, the present work provides a unified, sensorless, experimentally validated voltage-driven approach achieving both MPPT and power curtailment using only a boost converter, enhancing practicality and reproducibility.

To conclude, this state-of-the-art review has identified the following research gaps.

- Lack of control methods that enable both MPPT and power curtailment management by dynamically selecting the operating mode based on grid or system requirements. Existing approaches often focus exclusively on one objective.
- Power control strategies remain largely validated through simulation, with limited experimental verification in real SWTs, especially for power curtailment control.
- Existing methods often require non-standard SWTs topologies, relying on additional equipment such as sensors or auxiliary power converters.

These research gaps have been addressed by the contributions of this work, as presented in the next section.

1.2. Work contributions

Compared with previous studies, the contributions of this work are summarized below.

- A novel sensorless control methodology was developed that **enables both MPPT and power curtailment operation** based on an external command from the grid, user installation, or any upper control layer. The strategy allows seamless mode selection within a unified control framework while maintaining compatibility with existing controllers, without requiring additional power electronics or storage systems.
- A predefined lookup table (LUT) method was introduced to determine the reference voltage based on wind speed and power demand. This approach enables real-time voltage setpoint selection without requiring real-time learning, making it reproducible for other SWTs configurations.
- Design and implementation of a boost converter using a commercially available Half-Bridge IGBT module for SWTs applications.

1.3. Paper organization

The remainder of this paper is structured as follows. Section 2 introduces the WECS model, detailing the wind turbine, generator, and power electronics used in the study. Section 3 presents the proposed power control strategy, explaining the voltage-based regulation method and the implementation of the control system. Section 4 describes the simulation and experimental platforms developed for validation. Section 5 analyses the results obtained from both simulation and experimental tests, highlighting the system's performance and discussing its limitations. Finally, Section 6 summarizes the main conclusions and outlines potential future research directions.

2. Wind energy conversion model

The SWTs considered in this study (Fig. 1) consists of a wind turbine, a PMSG, a passive diode bridge rectifier, a DC–DC boost converter, and a DC bus. This configuration, based on a direct-drive topology with high power-electronic penetration, is widely adopted for small-scale systems due to its simplicity, low maintenance, and controllability.

The following subsections present the wind turbine, generator, and power converter models, establishing the theoretical basis for the proposed control strategy.

2.1. Wind turbine model

Wind turbines convert kinetic energy from wind into mechanical power, which is then transformed into electrical energy by the generator. The total wind power (P_w) available for extraction is given by Ref. [39]:

Table 1
Comparison of related works on power control in SWT.

Ref.	Control Objectives		Control Method	Complexity	Validation Type		Extra Hardware requirements[b]
	MPPT	PC[a]			Simulation	Experimental	
This work	✔	✔	cascaded PI control with LUT-based voltage reference	Low	✔	✔	None
[9]	✔	✘	P&O	Lox	✔	✔	Active Rectifier
[11]	✔	✘	Theoretical SWT model	Medium	✔	✔	None
[36]	✘	✔	Hierarchical control with PI-based cascaded voltage/current loops and droop control for reactive power	High	✔	✔	Inverter
[37]	✔	✔	Direct power control with adaptive PI	Medium	✔	✘	Inverter
[38]	✔	✔	Sliding-mode control	High	✔	✘	None

[a] Power Curtailment.
[b] Extra hardware requirements to archive the power control compared to the proposed work.

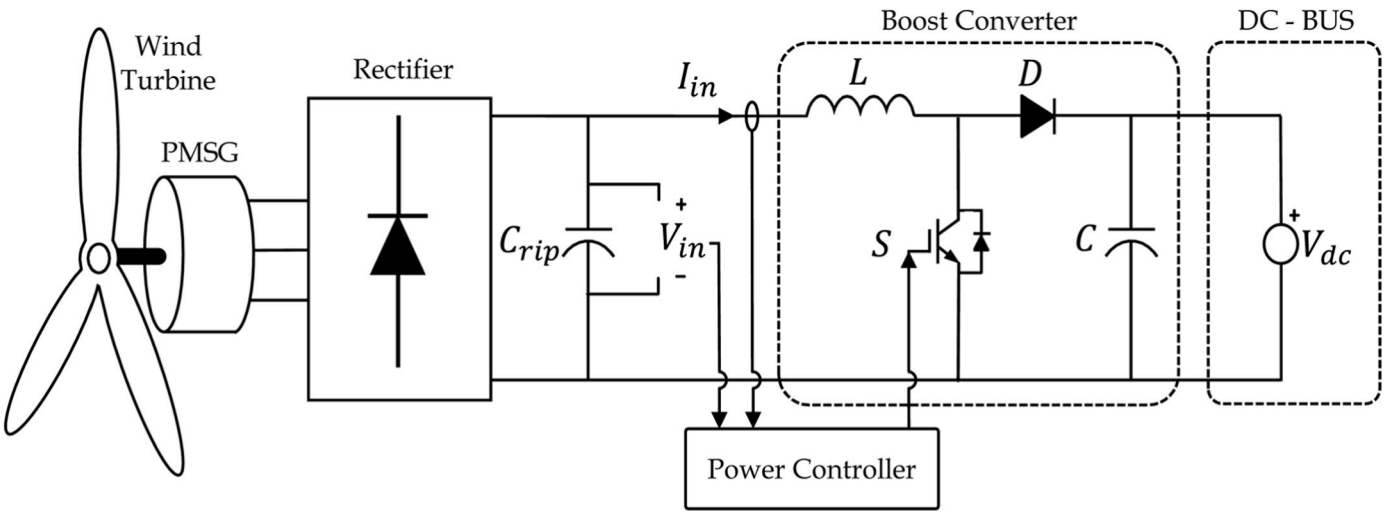

Fig. 1. Complete SWTs framework of this paper: wind turbine, PMSG, rectifier, DC/DC converter, DC bus and the power controller.

$$P_w = \frac{1}{2}\cdot\rho\cdot S\cdot v_w^3 \tag{1}$$

Where S is the surface area swept by the turbine blades, ρ is the density of the wind, and v_w is the wind velocity. However, only a fraction of this power can be effectively captured, defined by the power coefficient (C_P):

$$P_m = P_w\cdot C_P(\lambda,\beta) \tag{2}$$

Where $C_P(\lambda,\beta)$ depends on the tip speed ratio λ and the pitch angle β. The tip speed ratio is defined as [39]:

$$\lambda = \frac{R_b\cdot\omega_m}{v_w} \tag{3}$$

Where ω_m is the rotor speed and R_b the radius of the blades.

The optimizing of turbine efficiency is now contemplated in terms of maximising C_P by orienting the blades for each velocity of the wind. In SWTs, this feature (β) is established by the manufacturer and is invariable [40]. This reason leads to carry out a power control from the power electronic side, as explained in the state of art.

The turbine design determines $C_P(\lambda,\ \beta)$. Fig. 2 shows typical manufacturer-based power curves, where the red-shaded area illustrates the feasible power-regulation range below the maximum output for each wind speed.

The resulting mechanical power is:

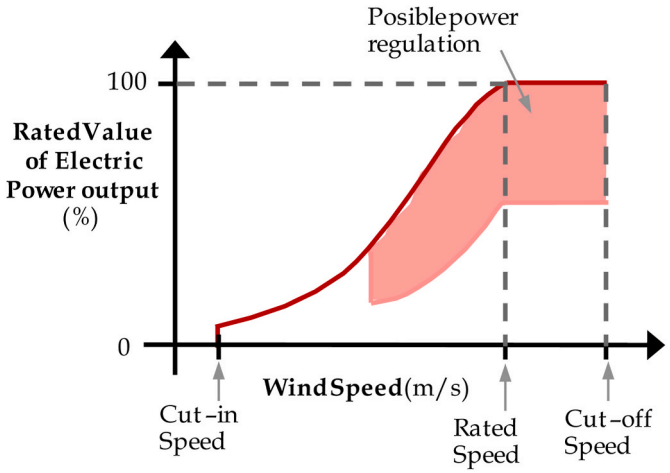

Fig. 2. Power coefficient and Power output for a standard small wind turbine.

$$P_m = \frac{1}{2}\cdot\rho\cdot\pi\cdot R^2\cdot v_w^3\cdot C_p(\lambda,\beta) \tag{4}$$

and the torque develop by the wind turbine is determined as follows:

$$T_m = \frac{P_m}{\omega_m} \tag{5}$$

In the presented wind conversion system, the torque generated by the wind turbine is directly transferred to the generator shaft, due to the absence of gearboxes or other transmissions mechanisms.

2.2. Permanent magnet synchronous generator model

In order to describe and model the PMSG electrical behaviour, the equations in the rotor d-q reference frame [41] are expressed as:

$$\begin{aligned}\frac{d}{dt}i_d &= \frac{1}{L_d}v_d - \frac{R}{L_d}i_d + \frac{L_q}{L_d}p\omega_m i_d \\ \frac{d}{dt}i_q &= \frac{1}{L_q}v_q - \frac{R}{L_q}i_q + \frac{L_d}{L_q}p\omega_m i_d - \frac{\phi p\omega_m}{L_q}\end{aligned} \tag{6}$$

Where v_d , v_q i_d and i_q, are the voltages and currents in the d − q reference frame, R and L characterize the resistance and inductance of the stator winding (in axes d and q), ϕ is the magnitude of the flux generated by the rotor's permanent magnets in the stator phases. The electromagnetic torque (T_e) can be determined and simplify as follow [41]:

$$T_e = 1.5p\lambda i_q + 1.5pi_d i_q\left(L_d - L_q\right) \rightarrow T_e = 1.5p\lambda i_q \tag{7}$$

T_e can be simplified since the reluctance effect is negligible ($L_d \approx L_q$).

The fundamental equation of dynamics for an electromechanical system can be now presented by putting to use equations (4), (5) and (7):

$$J\frac{d\omega}{dt} = T_m - T_e = \frac{\frac{1}{2}\rho\pi R^2 v_w^3 C_p}{\omega_m} - 1.5p\lambda i_q \tag{8}$$

where T_m is the mechanical torque and J is the total moment of inertia of the rotating mases.

Equation (7), accompanied by (6), describes the electromechanical interaction between the wind turbine and the generator, establishing a direct link between wind power extraction, generator speed, and electrical torque. This formulation supports the proposed voltage-based power regulation approach by providing an analytical framework to verify the steady-state power output for each imposed voltage reference, ensuring consistency with the experimental LUT-based control strategy

proposed in this work.

Since the system lacks active mechanical control, power regulation is achieved by modifying the generator load via the power converter. This influences the rotor speed (ω_m), affecting the generated voltage:

$$V_{generator} = k \cdot \phi \cdot \omega_m \rightarrow \frac{V_{generator}}{\omega_m} = const \tag{9}$$

Where $V_{generator}$ is the voltage generated by the machine, k is a constant related to generator properties. The simplification done in (10) can be assumed because during the regular operation of the machine k and ϕ remain constant. This relationship enables voltage-based control, where power extraction is regulated through the converter, eliminating the need for direct speed measurement. Hence, the proposed method operates in a fully sensorless manner with respect to the electromechanical subsystem, relying solely on electrical variables available at the converter terminals. The next section details the boost converter's role in implementing this strategy.

2.3. Power converter model

The power electronic interface between the generator and the DC bus consists of a boost converter, which regulates the rectified generator voltage (V_{in}, Fig. 1) to match a reference voltage (V_{ref}) defined by the control system. The boost converter follows the standard steady-state voltage relationship:

$$V_{DC\ bus} = \frac{V_{in}}{1 - D} \tag{10}$$

where D is the duty cycle and define the fraction of time the switching device remains ON. Since $V_{DC\ bus}$ is externally imposed and constant, the control variable is V_{in}, which is set according to the reference voltage V_{ref}. Given equation (10) and the fact that:

$$V_{in} = V_{generator} = K \cdot \omega_m \tag{11}$$

The voltage reference V_{ref} is determined from a LUT based on the desired power extraction level, that will be explained in the next section. Finally, the required duty cycle is computed as:

$$D = 1 - \frac{V_{ref}}{V_{DC\ bus}} \tag{12}$$

By dynamically selecting V_{ref}, the converter adjusts the electrical load seen by the generator, allowing power regulation without requiring additional mechanical control elements.

3. SWTs characterization based on LUT

To implement the control proposed, a characterization of the wind turbine is required [42]. Experimental measurements of power generation at different wind speeds and imposed voltages are used to construct a LUT, as shown in Table 2. This LUT provides a direct correlation between wind speed, generator voltage, and output power, enabling real-time selection of the reference voltage (V_{ref}).

Table 2
Look-up table: active power corresponding to different wind speeds and imposed voltages.

Voltage (V) \ Wind speed (m/s)	v_1	v_2	v_3	v_4	⋯	v_N
$\mathbb{V}_1$	P_{11}	P_{12}	P_{13}	P_{14}	⋯	$P_{\mathbb{V}_1 v_N}$
$\mathbb{V}_2$	P_{21}	P_{22}	P_{23}	P_{24}	⋯	$P_{\mathbb{V}_2 v_N}$
$\mathbb{V}_3$	P_{31}	P_{32}	P_{33}	P_{34}	⋯	$P_{\mathbb{V}_3 v_N}$
⋮	⋮	⋮	⋮	⋮	⋱	⋮
$\mathbb{V}_N$	$P_{\mathbb{V}_N v_1}$	$P_{\mathbb{V}_N v_2}$	$P_{\mathbb{V}_N v_3}$	$P_{\mathbb{V}_N v_4}$	⋯	$P_{\mathbb{V}_N v_N}$

$P_{\mathbb{V}_N v_N}$ shown in Table 2 is the output electrical power by the wind generator with the wind speed

v_N and the voltage imposed $\mathbb{V}_N$ as reference (V_{ref}).

Since the dataset is obtained through discrete measurements, a polynomial approximation is employed to ensure a continuous mapping of wind turbine behaviour. Using the *polyfit* function in MATLAB, a third-order polynomial function is fitted to the experimental data for each tested wind speed. This allows for the derivation of an analytical voltage-power relationship at each discrete wind speed.

The fitting degree was selected based on the minimum root mean square error (RMSE) across all data points.

For wind speeds not directly tested, interpolation methods are applied using the *griddata* MATLAB function. Among the available options, cubic interpolation was selected, as it produced smoother transitions and minimized discontinuities in the V_{ref} surface, as verified through visual inspection of the 3D power surface (Fig. 3).

Fig. 3 provides a 3D surface representation of the LUT dataset.

For a given wind speed v_x, imposing a voltage $\mathbb{V}_A$ results in a power output of P_A, corresponding to MPPT operation. However, for power curtailment operation, the reference voltage $\mathbb{V}_B$ is selected, reducing power extraction to P_B as dictated by the upper-layer power control manager.

4. Power control strategy

The power control strategy regulates the SWTs operation by dynamically adjusting the input voltage of the boost converter, thereby modifying the generator's electrical load. This approach enables both MPPT and power curtailment control, ensuring adaptability in grid-connected and standalone (isolated) operation.

- In grid-connected mode, the system adjusts power injection based on grid requirements, supporting ancillary services by modulating active power output.
- In standalone mode, the control strategy ensures that the load demand is met, regulating power extraction accordingly.

The control methodology follows three main stages.

4.1. Operation mode selection

The controller can operate under three distinct modes.

1. **Mode 1**: Extracting the maximum power available in the wind for any value of wind speed (variable speed), imposing the corresponding optimal voltage. **This mode is known as MPPT.**
2. **Mode 2**: Maintaining a predetermined percentage of power curtailment for any wind speed. **This mode ensures always a power availability when required.**
3. **Mode 3**: Regulating the active power delivered by the generator for any wind speed, provided that the requested power is available. **This mode enables precise power control,** allowing the system to adapt to external power demands.

The selection of the controller's operating mode is determined by the percentage of power reserve ($\%_{reserve}$) set by the upper-layer power control (P_{MAX}), see Fig. 4. If $\%_{reserve} = 0$, the system operates in Mode 1 (MPPT), extracting the maximum available power from the wind. If $\%_{reserve}$ is constant, the system maintains a fixed power reserve, corresponding to Mode 2. In contrast, if $\%_{reserve}$ varies dynamically based on the maximum power reference (P_{MAX}), the system operates in Mode 3, continuously adjusting power output according to external demands. This dynamic selection mechanism ensures flexibility in adapting to

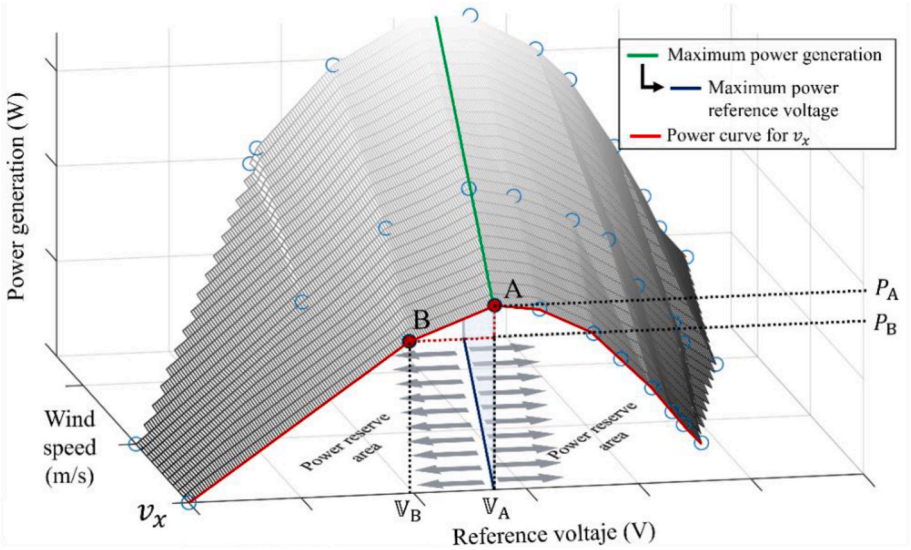

Fig. 3. Surface plot from SWTs characterization example.

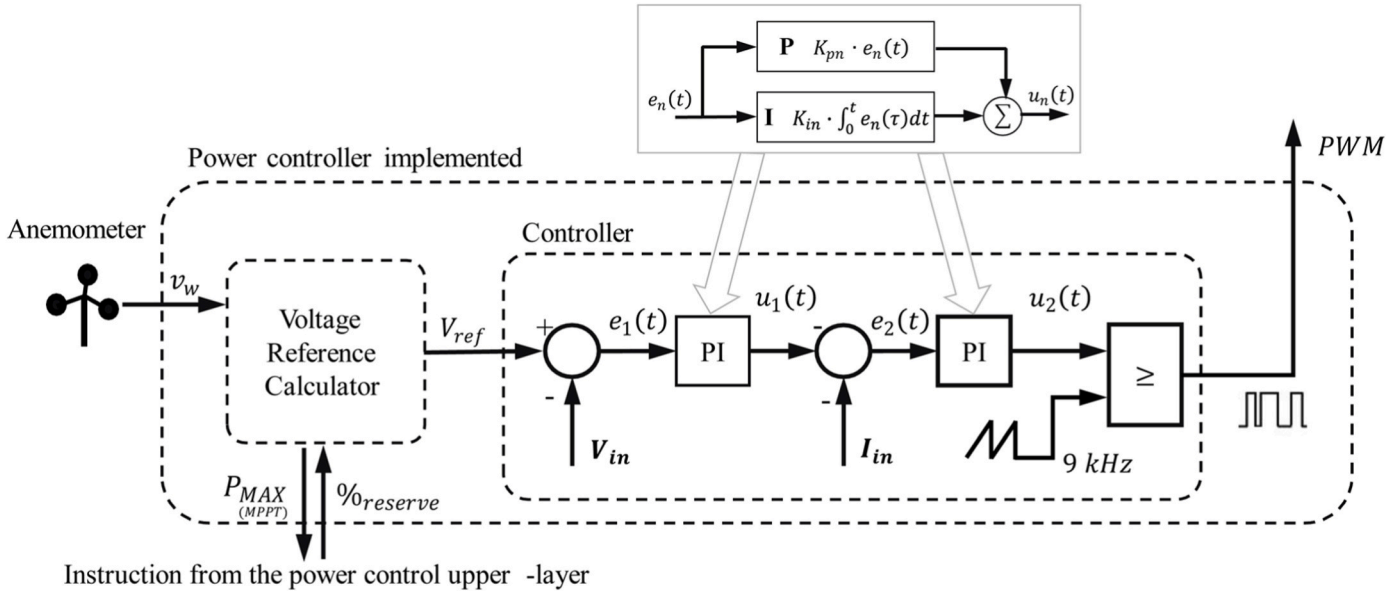

Fig. 4. Power controller structure.

different operational requirements. Fig. 4 illustrates the controller architecture.

4.2. Voltage reference calculation, V_{ref}

The reference voltage V_{ref} is dynamically determined based on the desired power extraction level. This process relies on the previously characterized LUT which correlates incident wind speed, generator voltage, and output power. By selecting an appropriate operating point, the system ensures compliance with either MPPT or power curtailment operation, depending on external control requirements.

Mathematically, V_{ref} is a function of the measured wind speed v_w and the desired power curtailment percentage:

$$V_{ref} = f(v_w, \%_{reserve}) \tag{13}$$

The calculated V_{ref} defines the input voltage of the boost converter, thereby indirectly regulating the electrical load seen by the generator. This control mechanism leverages Pulse Width Modulation (PWM) to adjust the duty cycle D (Equation (12)), modifying the energy transfer process and ensuring that the generator operates at the imposed voltage reference.

4.3. Controller implementation

The implemented controller consists of two cascaded proportional-integral (PI) controllers, as illustrated in Fig. 4. The outer voltage loop regulates V_{in} to match V_{ref}, while the inner current loop enhances the dynamic response by controlling the inductor current (I_{in}). The control structure is defined by the following equations:

$$\begin{aligned} e_1(t) &= V_{ref} - V_{in}(t) \\ u_1(t) &= K_{p1} e_1(t) + K_{i1} \int e_1(t)dt \end{aligned} \tag{14}$$

where $e_1(t)$ represents the voltage error, and $u_1(t)$ is the control output from the outer loop, which acts as a reference for the inner loop.

The inner loop is responsible for current regulation:

$$e_2(t) = -u_1(t) - I_{in}(t)$$
$$u_2(t) = K_{p2}e_2(t) + K_{i2}\int e_2(t)dt \quad (15)$$

Where $e_2(t)$ denotes the current error, and $u_2(t)$ is the modulating signal used to generate the PWM signal that drives the boost converter switch at the stablished switching frequency. Moreover, K_p and K_i are the proportional and integral gain for each PI.

Despite the widespread use of cascaded PI controllers in power electronics applications, this control structure remains well-suited for the proposed strategy. The novel contribution of this work lies in the methodology for dynamically selecting the desired power output by adjusting the voltage reference through a pre-characterized LUT. Given that the system operates under a well-defined and stable dynamic response, the PI-based architecture ensures a sufficient balance between implementation simplicity, robustness, and control accuracy, without necessitating more complex nonlinear or adaptive control techniques.

The PI controller parameters (K_{p1}, K_{i1}, K_{p2}, K_{i2}) were initially determined analytically based on the small-signal model of the boost converter. The voltage and current loops were designed using the classical frequency-response method, setting the inner current loop bandwidth approximately one decade higher than that of the outer voltage loop to ensure proper dynamic decoupling. The proportional and integral gains were then fine-tuned empirically through simulation to minimize overshoot. The final tuned values used in both the simulation and experimental platforms are listed in Tables 5 and 6 of the Appendix.

5. Simulation and experimental platforms

The proposed control strategy has been validated through both simulation and experimental implementation. Initially, the system was tested using MATLAB/Simulink to assess its theoretical performance. Subsequently, a laboratory prototype was developed to experimentally validate the control methodology under real operating conditions. The details of each implementation are presented in the following subsections.

5.1. Simulation platform

The simulation platform was built in MATLAB/Simulink, as illustrated in Fig. 5, following the wind turbine model and power converter topology previously described. A 3 kW horizontal-axis small wind turbine has been modelled based on reference [43], with its nominal parameters summarized in Table 3.

The wind turbine characteristics follow the same power curve representation as Fig. 2, ensuring consistency with real operational behaviour. Since the pitch angle is fixed by the manufacturer, the turbine inherently operates at maximum aerodynamic efficiency (MPPT mode) unless an external power curtailment is imposed. Thus, the proposed control strategy allows for selective deviation from MPPT to meet external power dispatch requirements.

To simulate the electrical generator behaviour, Simulink's PMSG block has been employed, parameterized using the default configuration corresponding to: "02: 1.7 Nm, 300 Vdc, 3750 RPM - 1.7 Nm."

A universal bridge rectifier is used to model the diode bridge rectification stage, with a capacitor placed to smooth voltage ripples. The boost converter is implemented using an inductor (L), an IGBT as the switching device controlled by the signal [u], and a capacitor (C). The values for L and C are detailed in Table 5 (Appendix). The system is connected to a DC bus maintained at 350 V, ensuring a stable operating environment for the power electronics.

Table 3
Nominal parameters of the wind turbine used in the simulation platform.

Datasheet Characteristics	Value	Unit
P_{nom}	3000	W
$C_{p,max}$	0.41	–
v_{nom}	12	m/s
v_{cutin}	2	m/s
v_{cutoff}	15	m/s

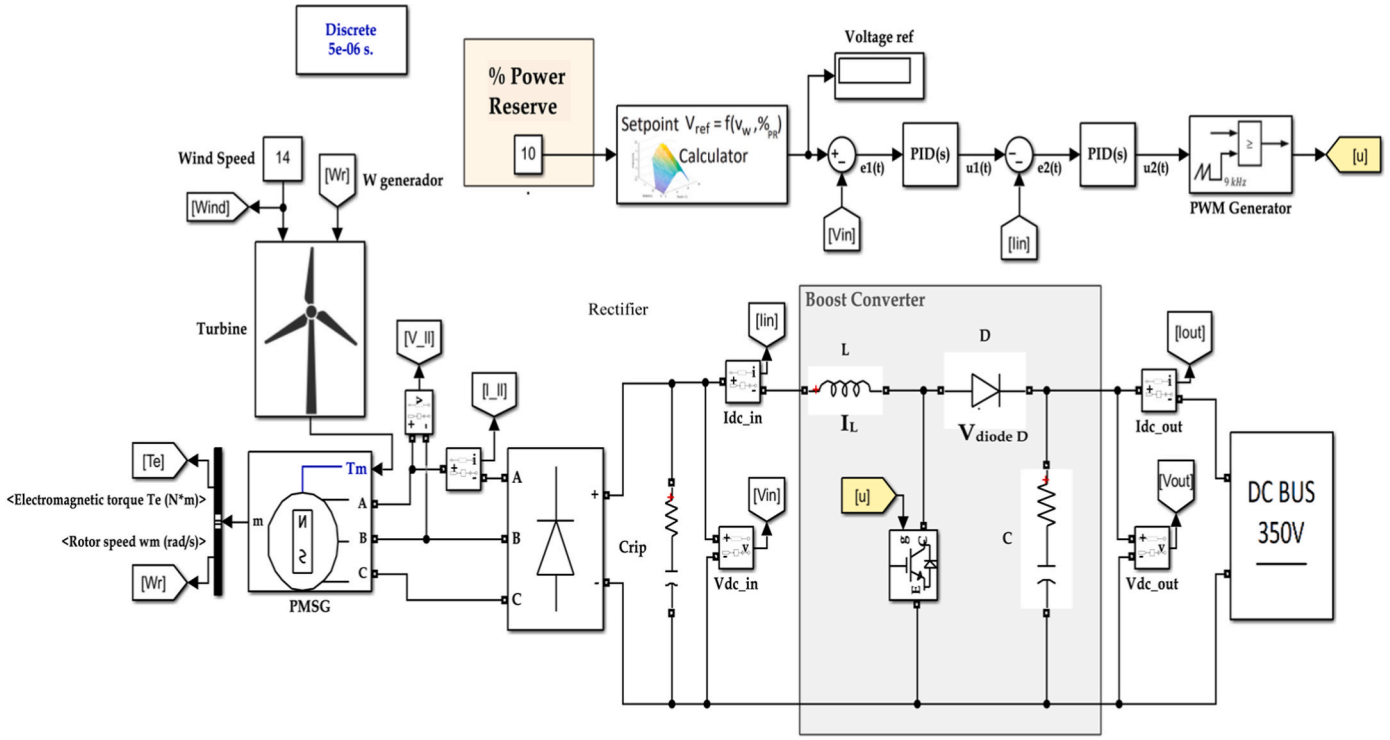

Fig. 5. Simulation platform developed to validate the control system.

5.2. Experimental platform

The experimental validation was performed using a hardware implementation of the complete SWTs, following the same system architecture as Fig. 1. The laboratory setup, depicted in Fig. 6, employs a commercial small wind turbine (FM910-4 MARLEC) manufactured by Rutland Windcharger. The turbine characteristics align with those described in Fig. 2, with cut-in and cut-off wind speeds of 3 m/s and 20 m/s, respectively. The maximum laboratory power output does not exceed 17.2 W. The nominal parameters of the turbine are provided in Table 6 (Appendix).

To emulate variable wind conditions, a motor-driven centrifugal fan controlled by a frequency converter was used. This setup allows for precise control of the incident wind speed on the turbine, enabling reproducible experimental conditions. For AC-to-DC conversion, a three-phase full-wave rectifier is employed, followed by a capacitor C_{rip} .

A modular IGBT power stack was integrated to built the boost converter, the internal scheme of this device is represented in Fig. 7 a) and its external appearance in Fig. 7 b). As can be observed from the available details, the power module incorporates the IGBT switch T1 always open is used as diode and IGBT switch T2 driven by the controller signal. Moreover, the module brings built-in the capacitor C. The parameters are shown in Table 6 of the appendix.

The output of the converter is connected to a battery that imposes a voltage of 350 ± 0.5 V. The battery has been emulated using a bi-directional source of direct current in battery-emulator Li-Ion mode, model PSB 9000 3U develop by the company EA Elektro Automatik. This has been the method to emulate a DC bus in lab.

By emulating the DC bus in this way, versatility, control, repeatability, and safety are achieved, which justifies its use in technical experiments.

The control strategy is implemented using an Arduino-based platform, following the architecture described in Fig. 4. The input voltage and current to the converter are measured using a dedicated PCB. The measurement setup involved the utilization of a non-invasive current sensor (LEM LA 55-P) and a voltage sensor (LV 25-P), and their respective signals were fed into the controller. The PWM generated by Arduino is the signal that govern T2, Fig. 7 a).

6. Results of the proposed power control strategy

Once the systems used for simulation and experimentation have been presented, this section analyses the substantial results in detail, those that serve to validate the control system proposed in this paper. The limitations and differences between models will also be discussed.

6.1. From simulation

From the simulation results, the key aspects analysed were the impact of voltage regulation on power extraction and the stability improvements provided by the closed-loop control.

The system was tested under varying wind speeds to analyse the relationship between imposed voltage and power curtailment levels. Fig. 8 shows, for each tested wind speed v_w, the power reserve $P_{reserve}(V_{ref}, v_w) = P(V_{ref}, v_w)/P_{\max}(v_w)$ as a function of the imposed generator voltage V_{ref}. This ratio, expressed as a percentage, represents the fraction of the maximum available power extracted at each operating voltage. Each colored curve corresponds to a different wind speed (see legend). These curves confirm that by decreasing the reference voltage, the extracted power is reduced, demonstrating the feasibility of the LUT-based power regulation strategy described in previous sections. By interpolating the power curtailment across different wind speeds, the simulation framework allows us to predefine the voltage reference V_{ref} required to meet a specific power curtailment setpoint.

Beyond confirming the effectiveness of voltage-based power regulation, the simulation study also evaluates the role of closed-loop control in stabilizing the system's electrical behaviour. Fig. 9 compares the input current waveforms obtained under two control schemes: Open-loop control, where only the reference voltage is imposed without feedback regulation and Closed-loop control, using a cascaded PI controller to regulate the generator voltage dynamically.

The open-loop configuration exhibits significant current oscillations,

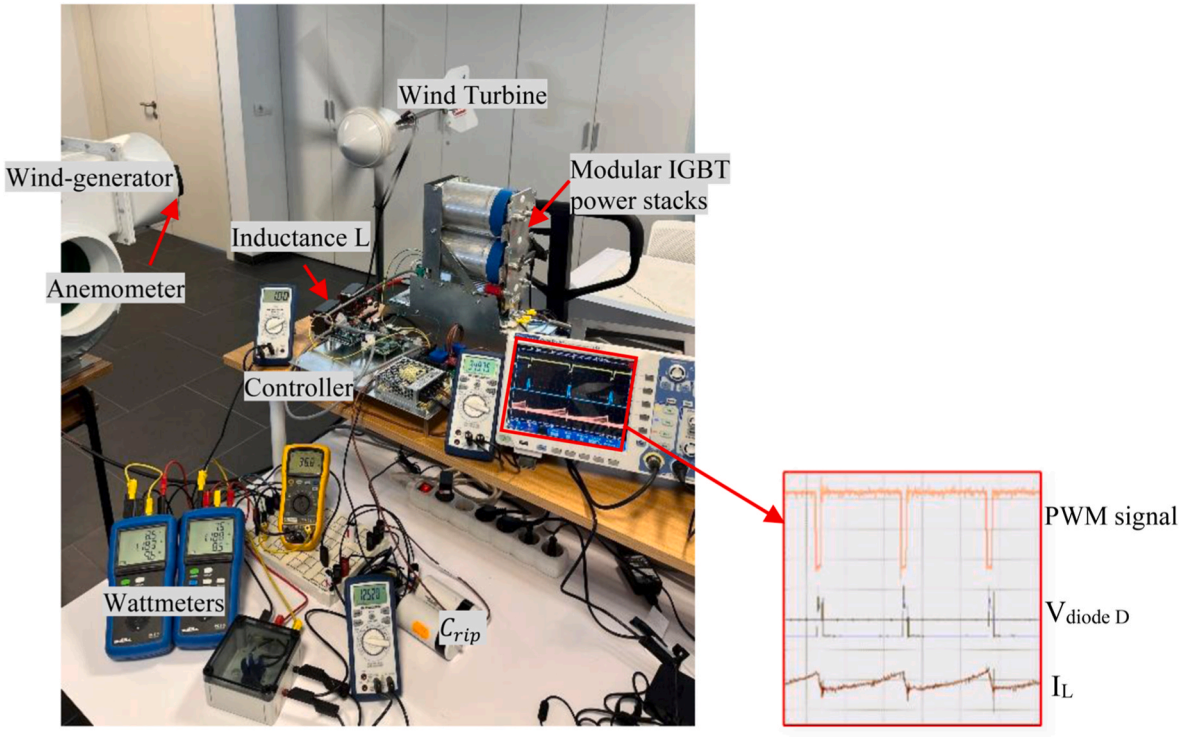

Fig. 6. The complete experimental SWTs.

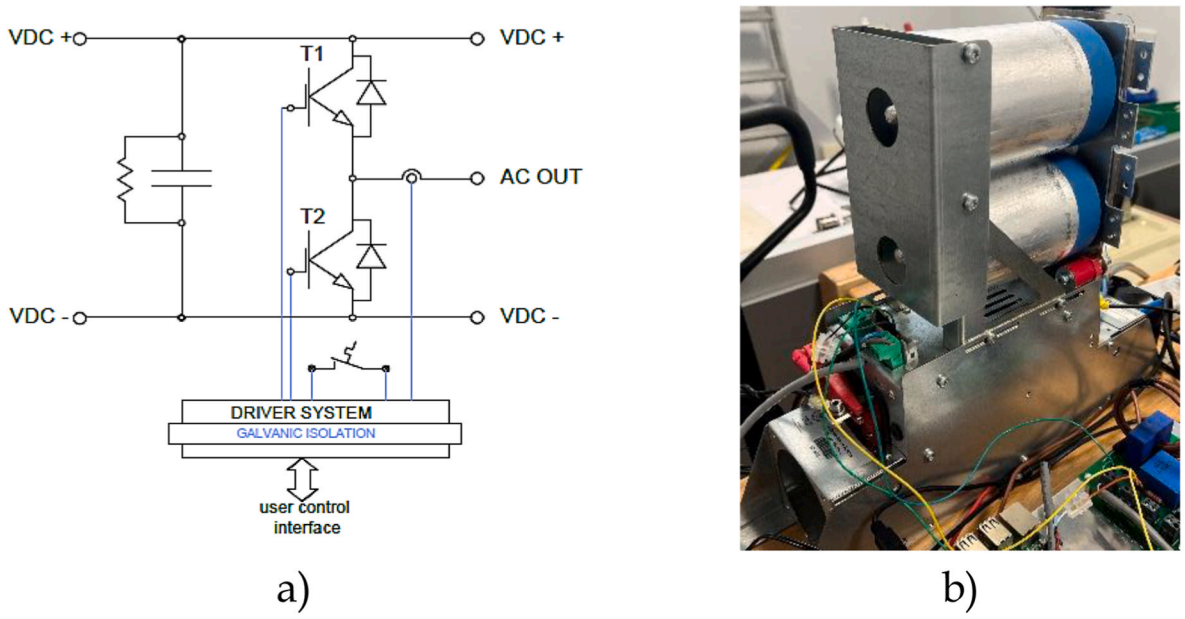

Fig. 7. DC/DC boost converter: a) structure, b) appearance.

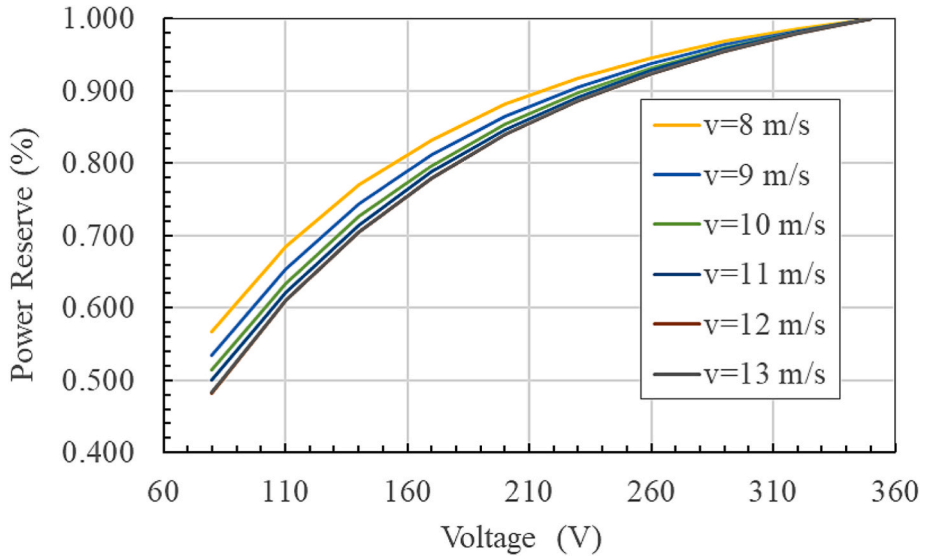

Fig. 8. Power reserve $P_{\text{reserve}}(V_{\text{ref}}, v_w) = P(V_{\text{ref}}, v_w)/P_{\max}(v_w)$ (%) obtained from simulation tests for $v_w = 8, 9, 10, 11, 12,$ and 13 m/s. Each curve represents a different wind speed.

leading to inefficient power conversion and a highly unstable electrical response. Conversely, the closed-loop PI controller mitigates these fluctuations, ensuring a smoother current profile and improving overall system robustness. These results highlight the necessity of implementing a feedback control loop, particularly when operating under variable wind conditions where power fluctuations are inevitable.

6.2. From experimental

The experimental validation aimed to confirm the feasibility of the proposed voltage-based control strategy in a real-world setting.

The power-voltage curves obtained from the experimental platform are presented in Fig. 10. These 2D curves represent the generated power as a function of the imposed generator voltage for different wind speeds. The results were obtained following the same LUT-based characterization methodology described previously in Section 3.1. The trends confirm that: for each wind speed, there exists an optimal voltage at which the maximum power is extracted. Moreover, when reference voltage is different from that optimal voltage, the extracted power decreases, validating the control principle behind the LUT approach.

Fig. 10 also includes two X-axes: the lower axis corresponds to the generator voltage, whereas the upper axis represents the rotor speed. As previously established in Equation (9), the voltage is directly proportional to the rotor speed in a PMSG, meaning that controlling the generator voltage effectively governs its mechanical speed.

To extend this characterization and enable real-time power regulation, the power-voltage relationship was reconstructed as a 3D surface, illustrated in Fig. 11. This surface presents the active power supplied by the generator for each wind speed and imposed generator voltage, serving as the reference framework for the Arduino-based controller.

The evaluation of the controller under operating Modes 1 and 2 is shown in Fig. 12. In Mode 1 (MPPT), Fig. 12 a), the system adjusts the

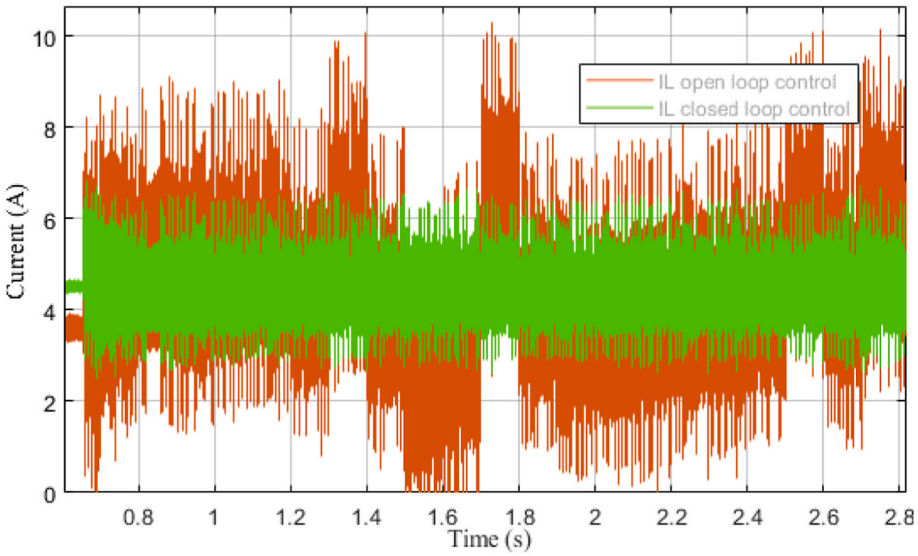

Fig. 9. Comparative noise analysis of Open and Closed Loop Control System.

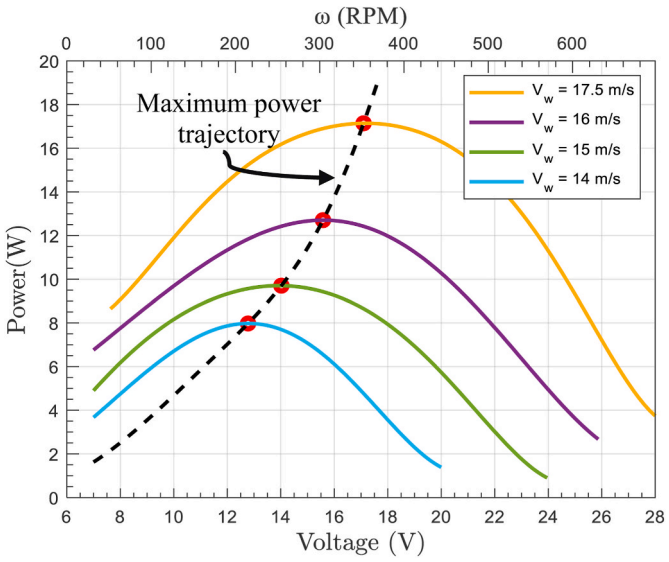

Fig. 10. Curves obtained from the experimental platform.

generator voltage to follow the maximum power curve for any incident wind speed, confirming the correct tracking of the optimal voltage reference. In Mode 2, Fig. 12 b), the controller maintains a fixed percentage of power reserve, operating below the maximum power trajectory according to the imposed curtailment level.

Each test was performed under controlled wind conditions generated by the laboratory fan, with the incident speed varying between 13.5 m/s and 18 m/s according to the sequence indicated in the figures. In Fig. 12 (a), corresponding to Mode 1 (MPPT), the generated electric power follows the variations in wind speed, showing four operating intervals at approximately 15 m/s, 16 m/s, 17.5 m/s and 15 m/s. A detailed view highlights the highest transient produced by the change from 16 m/s to 17.5 m/s, where the power signal reaches steady state after approximately 4.32 s. Fig. 12 (b) represents the operation in Mode 2, where the system was commanded to maintain fixed curtailment levels of 50 % and 20 % with respect to the maximum theoretical power. The complete experiment lasted about 510 s, with successive wind speed changes introduced to verify the controller behavior under the same environmental sequence as in Mode 1.

The control approach was further evaluated through a step-response test, where the controller was instructed to transition between different power setpoints while maintaining a constant wind speed of 17.5 m/s. This assessment was conducted with the controller operating in Mode 3,

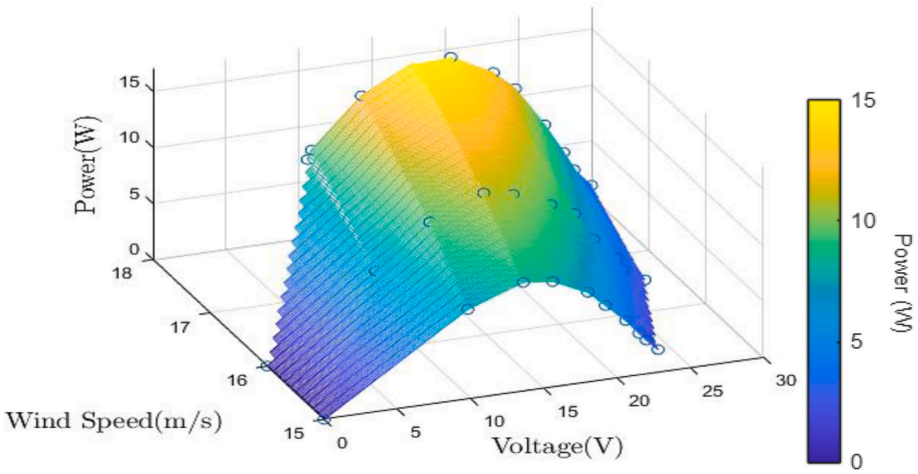

Fig. 11. Surface operation derived from experimental Data-Driven analysis.

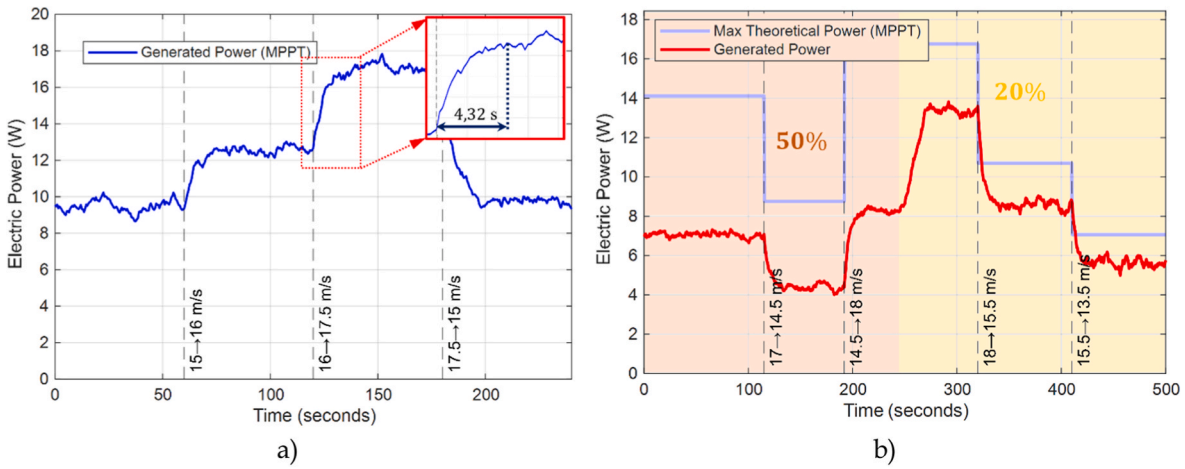

Fig. 12. Experimental results of the voltage-based control under different operation modes: a) Mode 1 – MPPT operation and b) Mode 2 – Constant power-reserve operation.

regulating the power reference dynamically. This test was selected as it represents the most demanding scenario, requiring the system to precisely regulate power output despite variations in the imposed setpoints.

The graphics results, presented in Fig. 13, demonstrate that the controller successfully tracks the imposed power levels (dashed lines in Fig. 13), with the power response aligning with the expected setpoints derived from Fig. 11.

The analytical results corresponding to this test are also presented in Table 4, where the response time/stability is explicitly calculated. Voltage reference, power delivered and the corresponding power curtailment (%) are also indicated for each set point value. The longest response time, 8.663 s, corresponds to the transition from 14.9 W to 8.4 W, primarily influenced by the combined effect of controller transients and turbine inertia.

The Time Response values in Table 4 represent the duration required for the output power to settle around the new reference level after each command issued by the upper-layer controller. Once the steady state is reached, small oscillations are observed in the measured power signal due to both the intrinsic dynamics of the PI controller and the aerodynamic fluctuations of the turbine.

The amplitude of these oscillations depends on the imposed operating voltage, as the converter exhibits slightly different dynamic behaviour at each voltage level. In all tested cases, the steady-state deviation with respect to the commanded reference remains below ±3 %. A moderate overshoot can be observed in the transient intervals. This behaviour is consistent with the selected PI tuning, which prioritizes fast dynamic tracking over overshoot minimization. The resulting transient performance represents a practical balance between response speed and voltage stability, depending on the desired control objectives.

Table 4
Experimental SWTs response Fig. 13 ($v_w = 17.5$ m/s).

Electric power	Voltage reference	Power curtailment	Time Response
$P_{\max\,ref1} = 17\ W$	$V_{ref1} = 15.8\ V$	$\%_{PR} = 0\ \%$	$\Delta t_1 = 7.454\ s$
$P_{ref2} = 11.2\ W$	$V_{ref2} = 9.46\ V$	$\%_{PR} = 34.1\ \%$	$\Delta t_2 = 6.385\ s$
$P_{ref3} = 14.9\ W$	$V_{ref3} = 12.6\ V$	$\%_{PR} = 12.3\ \%$	$\Delta t_3 = 3.566\ s$
$P_{ref4} = 8.4\ W$	$V_{ref4} = 8.6\ V$	$\%_{PR} = 50.5\ \%$	$\Delta t_4 = 8.663\ s$

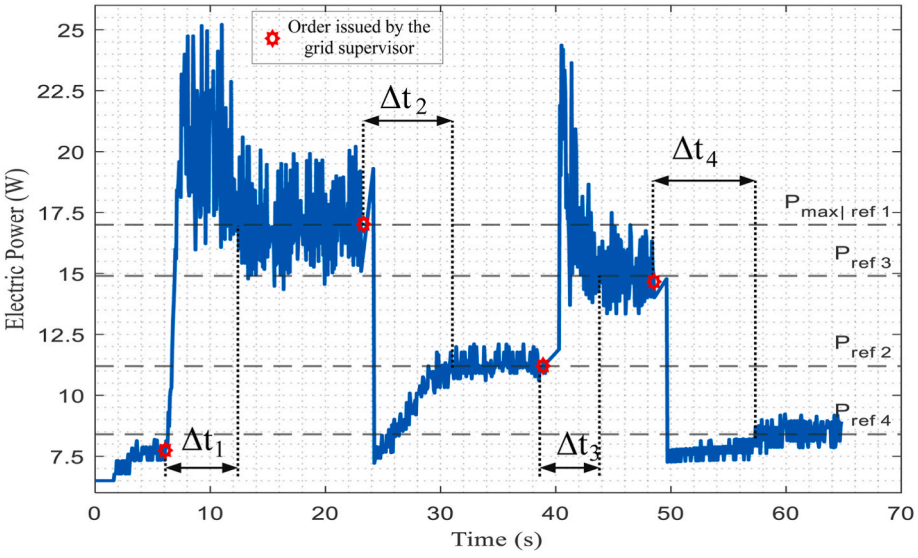

Fig. 13. Time response and stabilization of the voltage-based control to different % of power curtailment under mode 3 operation in a constant wind speed of 17.5 m/s.

6.3. Discussion and limitations

The experimental results are consistent with the simulation outcomes, reinforcing the feasibility of the proposed voltage-based control strategy. The tested WECS can operate at any desired point, whether at the maximum power point or a reduced power setpoint. Additionally, the implemented controller supports multiple operating modes, making the WECS highly versatile. Depending on the circumstances of its installation and operational requirements, the system can function in MPPT mode (Mode 1) to extract maximum power, in power curtailment mode (Mode 2) to ensure a controlled energy reserve at all times, or in grid-support mode (Mode 3) to regulate power delivery to the grid or a standalone load. This flexibility is particularly relevant in the context of modern power systems, where SWTs can provide ancillary services by dynamically adjusting their output based on grid demands.

However, some differences were identified between the simulation and experimental platforms, primarily due to the intrinsic differences between a modelled system and real-world conditions.

6.3.1. Discussion

One of the main discrepancies stems from the fact that the wind turbines used in simulation and experimentation have different power and speed characteristics. Consequently, their respective voltage, speed, and power curves exhibit notable variations. This divergence, however, does not undermine the validity of the study. The simulation was designed to validate a specific set of theoretical assumptions and control interactions, whereas the experimental validation sought to assess practical feasibility under real-world conditions. These complementary steps are essential for the progressive verification of the proposed control strategy.

Another significant factor influencing the results is the presence of non-idealities in the real system, such as voltage and current ripple, which are absent in the idealized simulation model. Additionally, the experimental turbine's power output was significantly lower than what would be expected under real outdoor conditions. This is primarily due to the artificial wind conditions in the laboratory environment, where the airflow is weaker, less stable, and subject to unwanted disturbances such as reflections and turbulence. In contrast, outdoor conditions typically provide a stronger and more stable wind flux. Nevertheless, these differences do not affect the validity of the control approach, as the study is fundamentally designed to compare different operating conditions rather than evaluate absolute energy yields.

Despite these differences, the fundamental principle of the proposed control strategy remains valid. The results confirm that SWTs can be effectively integrated into power curtailment strategies by utilizing a voltage-based control approach. The ability to impose a voltage reference to control power output ensures that the system can dynamically adapt to varying grid conditions and external demands, making it a valuable tool for renewable energy integration.

Regarding long-term operation, factors such as blade ageing, dirt accumulation, or aerodynamic degradation may slightly alter the power curve of the turbine. Since the proposed strategy operates as a voltage-driven loop, the system remains stable under these conditions. The controller will continue to enforce the reference voltage from the LUT, and while the operating point might slightly deviate from the theoretical new Maximum Power Point due to the curve shift, the system ensures continuous and safe operation without instability.

6.3.2. Limitations

The proposed control strategy is specifically designed for WECS that operate with PMSG, where the operating voltage is directly linked to the generated electromotive force. However, this approach would not be applicable to synchronous electromagnet generators, where voltage is regulated through an excitation current rather than being inherently tied to generator speed. In such cases, an entirely different control methodology would be required.

Although the generator tested in the laboratory operates at a low power level, the proposed control methodology remains fully scalable to higher power systems. The limiting factor in power scalability is not the generator itself but rather the power converter and its switching capabilities (i.e., the power–frequency constraints of the semiconductor devices). Given that the control system relies on fundamental machine principles, the proposed LUT-based methodology and control law remain unchanged and can be directly applied to larger WECS that maintain the same topological configuration (Fig. 1) tested in this work. Therefore, scaling up primarily involves adapting the converter hardware — including ratings, switching and thermal limits, and protection design — while the proposed control approach remains fully valid for higher power levels.

It is also noted that the transient response of the control system will vary depending on the rotational inertia of the wind turbine employed. Higher inertia generally results in smoother dynamic transitions and slower responses, while lower inertia yields faster but potentially more oscillatory behaviours. This effect can be accounted for during the control design phase to achieve a suitably damped and smooth transient response in each specific implementation.

Long-term effects such as ageing, dirt accumulation, or partial blade deterioration may slightly modify the turbine's aerodynamic characteristics. However, these variations can be detected through online monitoring and corrected by periodic recharacterization or control retuning, as discussed in Ref. [44].

7. Conclusions

This paper presents the development and implementation of a voltage-based power control strategy for small-scale wind turbines, allowing dynamic power adjustment between Maximum Power Point Tracking (MPPT) or power curtailment management. The method relies on a predefined Look-Up Table (LUT) to characterize the wind turbine's behaviour, establishing a direct correlation between wind speed, generator voltage, and electrical power output. This enables real-time selection of the optimal voltage reference based on the controller's operating mode to extract the desired power.

The proposed control strategy introduces three distinct operating modes: (1) MPPT mode, where the system extracts the maximum available power from the wind, (2) power curtailment mode, which maintains a predetermined percentage of power reserve, and (3) active power regulation mode, where the system dynamically adjusts power output based on external demands. The selection of these modes is dictated by the upper-layer power control, highlighting the adaptability and practical feasibility of the approach for different operational requirements, whether for grid support or standalone applications.

Both simulation and experimental validation confirm the feasibility and reliable performance of the proposed method. The results demonstrate that the system achieves fast and stable responses to power setpoint changes, ensuring smooth power regulation without the need for additional storage components. The cascaded PI-based control structure provides a simple yet robust mechanism to regulate power delivery by dynamically adjusting the boost converter's input voltage.

Future work will focus on developing predictive control techniques to enhance the dynamic response, as well as conducting extended outdoor validation to assess the system's robustness under stochastic wind conditions through statistical performance analysis.

CRediT authorship contribution statement

Jesus Clavijo-Camacho: Writing – original draft, Visualization, Software, Methodology, Investigation, Formal analysis, Conceptualization. **Reyes S. Herrera:** Writing – review & editing, Supervision, Project administration, Investigation, Funding acquisition, Conceptualization. **Francisco J. Ruiz-Rodriguez:** Writing – review & editing, Validation, Software, Investigation, Data curation. **Juan P. Torreglosa:** Writing –

review & editing, Software, Methodology, Investigation, Formal analysis.

Declaration of competing interest

The authors declare that they have no known competing financial interests or personal relationships that could have appeared to influence the work reported in this paper.

Acknowledgements

This research was supported by the grant PID2020-117828RB-I00 "Integral control system to optimize the microgrids energy demand" funded by MICIU/AEI/10.13039/501100011033 and, by "Spanish Ministry of Science, Innovation and Universities. In addition, the author Jesus Clavijo-Camacho is enjoying a INVESTIGO research fellowship funded by the European Union - NextGenerationEU. Funding for open access charge: Universidad de Huelva / CBUA.

Appendix

Table 5
Parameters of the SWT simulation model

PMSG 1.7 Nm 300 Vdc 3750 RPM - 1.7 Nm (Default Simulink Model) Rectifier	
C_{rip} DC-DC Boost Converter	16.7 mF
L C Controller parameters	83.3 mH 70.4 μF
K_{p1} K_{i1} K_{p2} K_{i2}	0.5 0.15 0.7 0.05

Table 6
Parameters of the experimental SWT

Wind Turbine	
No, of blades	6
Blades diameter	910 mm
Armature resistance	2.42 Ω
Stator inductance	0.0218 H
No, of poles	4
Rated power	160 W
Rectifier	
C_{rip}	99.25 mF
Diode $\text{Voltage}_{\text{threshold}}$	0.635 V
Controller parameters	
K_{p1}	0.3
K_{i1}	0.0012
K_{p2}	0.23
K_{i2}	0.01

Data availability

Data will be made available on request.

References

[1] Electricity from renewable sources reaches 47% in 2024». Accedido: 25 de marzo de 2025. [En línea]. Disponible en: https://ec.europa.eu/eurostat/web/products-eurostat-news/w/ddn-20250319-1.
[2] Renewable energy targets - European commission». Accedido: 25 de marzo de 2025. [En línea]. Disponible en: https://energy.ec.europa.eu/topics/renewable-energy/renewable-energy-directive-targets-and-rules/renewable-energy-targets_en..
[3] Study finds distributed wind energy potential equivalent to half of national electricity demand», Energy Gov. Accedido: 25 de marzo de 2025. [En línea]. Disponible en: https://www.energy.gov/eere/articles/study-finds-distributed-wind-energy-potential-equivalent-half-national-electricity.
[4] Gil-García IC, Fernández-Guillamón A, Montes-Torres y ÁH. Innovation in clean energy from man-made wind and small-wind generation. Sci Rep oct. 2024;14(1): 22932. https://doi.org/10.1038/s41598-024-74141-w.
[5] Hur S. Modelling and control of a wind turbine and farm. Energy 2018;156: 360–70. https://doi.org/10.1016/j.energy.2018.05.071. ago.
[6] Leary J, Schaube P, Clementi y L. Rural electrification with household wind systems in remote high wind regions. Energy Sustain Dev oct. 2019;52:154–75. https://doi.org/10.1016/j.esd.2019.07.008.
[7] Distributed wind market report: 2023 edition», Energy Gov. Accedido: 2 de noviembre de 2025. [En línea]. Disponible en: https://www.energy.gov/eere/wind/articles/distributed-wind-market-report-2023-edition.
[8] Artal-Sevil JS, Dufo R, Domínguez JA, Bernal-Agustín y JL. Small wind turbines in smart grids. Transformation of electrical machines in permanent magnet synchronous generators. In: en *2018 Thirteenth International Conference on*

Ecological Vehicles and Renewable Energies (EVER); 2018. p. 1–8. https://doi.org/10.1109/EVER.2018.8362404. abr.
[9] Nayanar V, Kumaresan N, Gounden y NA. A single-sensor-based MPPT controller for wind-driven induction generators supplying DC microgrid. IEEE Trans Power Electron feb. 2016;31(2):1161–72. https://doi.org/10.1109/TPEL.2015.2420568.
[10] Cisneros R, Mancilla-David F, Ortega y R. Passivity-based control of a grid-connected small-scale windmill with limited control authority. IEEE Journal of Emerging and Selected Topics in Power Electronics 2013;1(4):247–59. https://doi.org/10.1109/JESTPE.2013.2285376. dic.
[11] Urtasun A, Sanchis P, San Martín I, López J, Marroyo y L. Modeling of small wind turbines based on PMSG with diode bridge for sensorless maximum power tracking. Renew Energy jul. 2013;55:138–49. https://doi.org/10.1016/j.renene.2012.12.035.
[12] Narayana M, Putrus GA, Jovanovic M, Leung PS, McDonald y S. Generic maximum power point tracking controller for small-scale wind turbines. Renew Energy ago. 2012;44:72–9. https://doi.org/10.1016/j.renene.2011.12.015.
[13] Thiringer P Chen y T. Analysis of energy curtailment and capacity overinstallation to maximize wind turbine profit considering electricity price-wind correlation. IEEE Trans Sustain Energy oct. 2017;8(4):1406–14. https://doi.org/10.1109/TSTE.2017.2682820.
[14] Zhao Y, Ye L, Wang W, Sun H, Ju Y, Tang y Y. Data-driven correction approach to refine power curve of wind farm under wind curtailment. IEEE Trans Sustain Energy ene. 2018;9(1):95–105. https://doi.org/10.1109/TSTE.2017.2717021.
[15] Oh J-S, Lee J-H, Kim y J-E. Rapid power curtailment method considering power imbalance of the wind power generation system. J Electr Eng Technol sep. 2024;19(7):3873–84. https://doi.org/10.1007/s42835-024-01963-z.
[16] Park y J, Law KH. Cooperative wind turbine control for maximizing wind farm power using sequential convex programming. Energy Convers Manag sep. 2015;101:295–316. https://doi.org/10.1016/j.enconman.2015.05.031.
[17] Messina R Lanzafame y M. Power curve control in micro wind turbine design. Energy feb. 2010;35(2):556–61. https://doi.org/10.1016/j.energy.2009.10.025.
[18] Xie J, Dong H, Zhao y X. Data-driven torque and pitch control of wind turbines via reinforcement learning. Renew Energy oct. 2023;215:118893. https://doi.org/10.1016/j.renene.2023.06.014.
[19] Joo RP Antonysamy y YH. Power maximization and regulation of the super-large wind turbine system using generalized predictive approach-based torque and pitch control. Int J Electr Power Energy Syst 2023;154:109416. https://doi.org/10.1016/j.ijepes.2023.109416. dic.
[20] Wang Z, et al. Enhanced DC-link voltage control of PMSG-based wind turbine generators by machine-side converter during asymmetrical grid faults. Int J Electr Power Energy Syst 2024;155:109638. https://doi.org/10.1016/j.ijepes.2023.109638. ene.
[21] Sarsembayev B, Zhakiyev N, Kushekkaliyev A, Kayisli K, Do y TD. Output regulation-based optimal control system for maximum power extraction of a machine-side power converter in variable-speed WECS. IEEE Access 2024;12:8422–31. https://doi.org/10.1109/ACCESS.2024.3352546.
[22] Polinder H, Ferreira JA, Jensen BB, Abrahamsen AB, Atallah K, McMahon y RA. Trends in wind turbine generator systems. IEEE Journal of Emerging and Selected Topics in Power Electronics sep. 2013;1(3):174–85. https://doi.org/10.1109/JESTPE.2013.2280428.
[23] Higuchi Y, Yamamura N, Ishida M, Hori y T. An improvement of performance for small-scaled wind power generating system with permanent magnet type synchronous generator. In: en *2000 26th Annual Conference of the IEEE Industrial Electronics Society. IECON 2000. 2000 IEEE International Conference on Industrial Electronics, Control and Instrumentation*, vol. 2. 21st Century Technologies; oct. 2000. p. 1037–43. https://doi.org/10.1109/IECON.2000.972265.
[24] Freire y NMA, Cardoso AJM. Fault-tolerant PMSG drive with reduced DC-Link ratings for wind turbine applications. IEEE Journal of Emerging and Selected Topics in Power Electronics mar. 2014;2(1):26–34. https://doi.org/10.1109/JESTPE.2013.2295061.
[25] Chen Z, Guerrero JM, Blaabjerg y F. A review of the state of the art of power electronics for wind turbines. IEEE Trans Power Electron 2009;24(8):1859–75. https://doi.org/10.1109/TPEL.2009.2017082. ago.
[26] Beddar A, Bouzekri H, Babes B, Afghoul y H. Experimental enhancement of fuzzy fractional order PI+I controller of grid connected variable speed wind energy conversion system. Energy Convers Manag sep. 2016;123:569–80. https://doi.org/10.1016/j.enconman.2016.06.070.
[27] Zheng X, Feng Y, Han F, Yu y X. Integral-type terminal sliding-mode control for grid-side converter in wind energy conversion systems. IEEE Trans Ind Electron may 2019;66(5):3702–11. https://doi.org/10.1109/TIE.2018.2851959.
[28] Hashish MNA, Daoud AA, Elfar y MH. Hybrid MPPT-based predictive speed control model for variable speed PMSG wind energy conversion systems. Int J Appl Power Eng sep. 2022;11(3). https://doi.org/10.11591/ijape.v11.i3.pp218-228. Art. n.º 3.
[29] Shiravani F, Antonysamy RP, Mayilsamy G, Joo YH, Egiguren PA, Cortajarena y JA. Predictive PI control for maximum power point tracking and DC-Link voltage regulation of PMVG-based wind turbine systems. IEEE Journal of Emerging and Selected Topics in Industrial Electronics oct. 2024;5(4):1470–80. https://doi.org/10.1109/JESTIE.2024.3384090.
[30] Dreidy M, Mokhlis H, Mekhilef y S. Inertia response and frequency control techniques for renewable energy sources: a review. Renew Sustain Energy Rev mar. 2017;69:144–55. https://doi.org/10.1016/j.rser.2016.11.170.
[31] Ibrahim K Belmokhtar y H. A new reactive power management strategy to enhance the behavior of the wind turbine generator driven a DFIG under grid faults. In: en *2015* IEEE Electrical Power and Energy Conference (EPEC); oct. 2015. p. 16–21. https://doi.org/10.1109/EPEC.2015.7379920.
[32] Salles MBC, Cardoso JR, Grilo AP, Rahmann C, Hameyer y K. Control strategies of doubly fed induction generators to support grid voltage. In: en *2009 IEEE International Electric Machines and Drives Conference*; may 2009. p. 1551–6. https://doi.org/10.1109/IEMDC.2009.5075410.
[33] Engleitner R, Nied A, Matos Cavalca MS, da Costa y JP. Dynamic analysis of small wind turbines frequency support capability in a low-power wind-diesel microgrid. IEEE Trans Ind Appl feb. 2018;54(1):102–11. https://doi.org/10.1109/TIA.2017.2761833.
[34] Boyle J, Littler T, Foley y A. Battery energy storage system state-of-charge management to ensure availability of frequency regulating services from wind farms. Renew Energy nov. 2020;160:1119–35. https://doi.org/10.1016/j.renene.2020.06.025.
[35] Naz MN, Imtiaz S, Bhatti MKL, Awan WQ, Siddique M, Riaz y A. Dynamic stability improvement of decentralized wind farms by effective distribution static compensator. J Mod Power Syst Clean Energy may 2021;9(3):516–25. https://doi.org/10.35833/MPCE.2018.00422.
[36] Mastromauro RA, Orlando NA, Ricchiuto D, Liserre M, Dell'Aquila y A. Hierarchical control of a small wind turbine system for active integration in LV distribution network. In: en *2013 International Conference on Clean Electrical Power (ICCEP)*; jun. 2013. p. 426–33. https://doi.org/10.1109/ICCEP.2013.6587025.
[37] Dos Santos Neto PJ, Cecilio Pinto A, Dos Santos Barros TA, Ruppert Filho y E. A proposal to control active and reactive power in distributed generation systems using small wind turbines. IEEE Latin Am Trans oct. 2020;18(10):1699–706. https://doi.org/10.1109/TLA.2020.9387640.
[38] Senanayaka JSL, Karimi HR, Robbersmyr y KG. A novel soft-stall power control for a small wind turbine. In: en *2017* IEEE 26th International Symposium on Industrial Electronics (ISIE); jun. 2017. p. 940–5. https://doi.org/10.1109/ISIE.2017.8001372.
[39] Burton T, Jenkins N, Sharpe D, Bossanyi y E. Wind energy handbook. 2011.
[40] Salas-Cabrera R, et al. On the real time estimation of the wind speed for wind energy conversion systems. In: en *20TH INTERNATIONAL CONFERENCE ON ELECTRONICS COMMUNICATIONS AND COMPUTERS (CONIELECOMP 2010)*. New York: IEEE; 2010. p. 237–41. https://doi.org/10.1109/CONIELECOMP.2010.5440760. en International Conference on Electronics Communications and Computers CONIELECOMP.
[41] Yin M, Li G, Zhou M, Zhao y C. Modeling of the wind turbine with a permanent magnet synchronous generator for integration. In: en *2007 IEEE Power Engineering Society General Meeting*; jun. 2007. p. 1–6. https://doi.org/10.1109/PES.2007.385982.
[42] Clavijo-Camacho J, Gomez-Ruiz G, Ruiz-Rodriguez FJ, Sanchez-Herrera y R. A modular IGBT power stack – based and open hardware framework for small wind turbines assessment. Sustain Energy Technol Assessments jun. 2024;66:103804. https://doi.org/10.1016/j.seta.2024.103804.
[43] Ferrario AM, Vivas FJ, Manzano FS, Andujar JM, Bocci E, Martirano y L. Hydrogen vs. battery in the long-term operation. A comparative between energy management strategies for hybrid renewable microgrids. Electronics 2020;9(4):698. https://doi.org/10.3390/electronics9040698. abr.
[44] Clavijo-Camacho J, Gomez-Ruiz G, Sanchez-Herrera R, Magro y N. Remote real-time monitoring and control of small wind turbines using open-source hardware and software. Applied Sciences 2025;15(12):6887. https://doi.org/10.3390/app15126887. ene.